Research Square

Preprints are preliminary reports that have not undergone peer review.
They should not be considered conclusive, used to inform clinical practice,
or referenced by the media as validated information.

Synergistic impacts of plant growth promoting Pseudomonas geniculata TIU16A3 and green-synthesized iron-oxide nanoparticles from Eichhornia crassipes for the amelioration of heavy metal stress in Vigna radiata L.

Barkha Madhogaria
Techno India University
Sangeeta Banerjee
Techno India University
Sohini Chakraborty
Techno India University
Prasanta Dhak
Techno India University
Atreyee Kundu
atreyee.k@technoindiaeducation.com

Techno India University

Research Article

Keywords: Bioremediation, Vigna radiata L., Eichhornia crassipes, nanoparticle, Fe-O-NP, TIU16A3

Posted Date: September 5th, 2024

DOI: https://doi.org/10.21203/rs.3.rs-4863542/v1

License: This work is licensed under a Creative Commons Attribution 4.0 International License.
Read Full License

Additional Declarations: No competing interests reported.

Abstract

Plants are often affected by deleterious effects of heavy metals (HM). This HM stress leads to growth and production capacity issues. The most hazardous trace metals in agricultural areas are lead (Pb), cadmium (Cd), and chromium (Cr). It is not only carcinogenic to humans, but also negatively affects plants' phenotypic, biochemical, and genetic properties. Bioremediation can be used to economically remove contamination of heavy metals. The study aims to test the bioremediation potential of biogenic iron oxide nanoparticles (Fe-O-NP) along with *Pseudomonas geniculata* strain TIU16A3 (accession number OR507186). Plants of *Eichhornia crassipes* were used to create Fe-O-NP. Individually iron oxide nanoparticles exhibited enhancement of phenotypic traits in *Vigna Radiata* L. under heavy metal stress. We used four concentrations (10, 20, 40, and 80 mg/L) of Cr, Cd, and Pb for stress conditions. Biogenic nanoparticles and TIU16A3 in combination act synergistically with the increase in the amount of chlorophyll content and growth in distinct phenotypic traits. In plants, under HM stress, levels of antioxidant enzymes were observed to be high including superoxide dismutase, peroxidase, and catalase and H_2O_2 content and electrolyte leakage, when they were treated with biogenic NPs and TIU16A3 together the antioxidants decreased significantly. TIU16A3 and Fe-O-NP synergistically in the presence of Cd and Cr enhanced the expression of the *Aux/IAA* gene more than the expression observed in the presence of Fe-O-NP only. Due to the enhancement of intrinsic properties, and ability to remove Cr, and Cd by TIU16A3 when used in combination with Fe-O-NP for bioremediation exhibits promising results.

Highlights

- Nanoparticles are reported to aid in plant growth promotion and alleviate heavy metals and the sustainable approach of synthesizing potential iron oxide nanoparticles (Fe-O-NP) has been studied.
- Water hyacinth serves as a reducing and capping agent for the production of desired Fe-O-NP.
- Efficiency of TIU16A3 (accession number OR507186) and biogenic Fe-O-NP to bio-remediate soil contaminated with heavy metals have been first reported in the present study.
- Combinatorial strategy effect on the alleviation of heavy metal and growth of economically important legume *Vigna radiata* L. is a breakthrough research so far.
- Economical and sustainable eradication of water hyacinths by using them to produce non-toxic nanoparticles.

1. Introduction

The tanning process used in the leather industry uses chromium (Cr) and other hazardous chemicals. It is said that 80–90% of leather is tanned with basic chromium sulfate (BCS) and only 50–70% of Cr is fixed in chromium tanning; the remaining Cr is released into wastewater(Saravanabhavan et al. 2017). According to(Gupta et al. 2007), the leather industry is the largest producer of heavy metals in a nearby water facility. The sludge is also used for irrigation, which causes heavy metal (HM) contamination in agricultural land. When sludge is used for irrigation, heavy metals such as Cd, Zn, Cr, Ni, Pb, and Mn can

accumulate in surface soils and enter groundwater or soil solutions that can be taken up by plants(Mondal et al. 2017). Before the independence of West Bengal, three agglomerations of Kolkata - Tangra, Topsia, and Tilala - saw the activity of the leather industry. However, the leather industry moved about 20 kilometres from Kolkata to Bantala, where they are now located at the Calcutta Leather Complex (CLC). More than 300 tanneries moved to CLC due to the Supreme Court decision. CLC is supplied with a Common Effluent Treatment Plant (CETP), which uses several methods to treat a significant amount of wastewater from nearby tanneries before it is released back into the environment. Liquid and solid waste from tanneries and other factories entering water bodies adversely affects the natural ecosystem of the Ramasar area and can damage major waterways due to the 12,500-hectare East Kolkata Wetland adjacent to Bantala. It is generally known that heavy metal pollution negatively affects plant germination, photosynthesis, yield, and mineral nutrition (Kundu et al. 2019; Banerjee et al. 2023). When animals and humans eat plants contaminated with heavy metals, the metals are absorbed through the food chain into their cells and tissues can damage the intestinal microbiota and cause several chronic diseases in humans (Madhogaria et al. 2022). Heavy metals negatively affect dry matter, root and shoot growth (Naz et al. 2015). Many studies have shown that certain bacterial species can effectively promote bioremediation of metal-contaminated soil. *Pseudomonas* sp., *Enterobacter cloacae*, *Bacillus* sp., and other metal-resistant PGPBs are already been studied for the purpose (Zulfiqar et al. 2022). Biosorbents are one of the many technologies available to remove heavy metals from the environment(Banerjee et al. 2022; Madhogaria et al. 2024b). In recent decades, nanotechnology has become a central area of research. Researchers are paying more attention to a green approach to produce nanoparticles (NPs) without harming the environment by using an aqueous solution of plant extract. The effect of metal oxide nanoparticles on plants has been studied previously(Kiwumulo et al. 2022). Plant extracts contain sugars, terpenoids, polyphenols, etc. which can stabilize and reduce metal nanoparticles. Functional groups and phenolic compounds have been shown to contribute to the formation of metal nanoparticles. The International Union for Conservation of Nature (IUCN) has listed water hyacinth (*Eichhornia crassipes*) as one of the 100 most popular invasive and aggressive species that reproduce quickly. Under the right conditions, biomass can double in just a week, causing some problems for waterways. The green synthesis of Fe-O-NPs by *E. crassipes* has not yet been investigated, and the plant growth properties of these NPs have hardly been documented in the literature. Iron is oxidizable, so instead of reducing Fe^{2+} to FeO, the phytochemicals in the extract react with iron ions to form iron oxide nanoparticles. Iron oxide nanoparticles, or Fe-O-NPs, were chosen over other iron oxide phases due to their infrared, magnetic, and optical properties and stability. TEM, FTIR, UV-Vis spectroscopy, and X-ray diffraction confirm the morphology and presence of nanoparticles. Fe affects important physiological functions in plants, such as respiration, redox reactions, and chlorophyll production. In addition, the large surface area of Fe-O-NPs acts as a platform to reduce nutrient losses and ensure the timely delivery of nutrients to plants. Fe-O-NPs have recently been used directly to improve plant growth and alleviate drought stress and heavy metal pollution(Rizwan et al. 2019; Yang et al. 2020). Treatment of plants with Fe-O-NPs has also been studied in connection with the solubilization of heavy metals.

Agricultural applications of Fe-O-NPs are an exciting area of current research. Compared to other nanoparticles, Fe-O-NPs are toxic to soil bacterial communities. In addition, they support seed germination and maintain soil pH and nutrient levels(Rastogi et al. 2019). Previous studies have investigated how Fe-O-NPs can increase crop growth and yield by accelerating photosynthesis and altering several other metabolic processes. Although PGPR and Fe-O-NP have established distinct roles, little is known about their functions. Their small size and large surface area help them to cause strong adsorption of various molecules, which increases their effectiveness(Nayana et al. 2020). There are no studies on the synergistic and comparative use of Fe-O-NP and PGPR to reduce heavy metal stress in *Vigna radiata* L. There is a theory suggesting that PGPR and Fe-O-NP are important in stressed plants. This work aimed to investigate the relative and synergistic effects of heavy metal-resistant PGPR and Fe-O-NP isolated from tannery wastewater-affected soil on germination and growth of *V. radiata* L. under heavy metal stress, especially Cr and Cd.

2. Materials and Methods

2.1. Chemicals

The raw materials utilized in the production of Fe-O-NPs from *Eichhornia crassipes*, namely $Fe_2SO_4.7H_2O$ (98.5%), ethanol (99%), and NaOH (97%), were procured from LOBA CHEMIE PVT. LTD. *Eichhornia crassipes*, utilized herein, were procured from the pond site situated near Techno India University in West Bengal. Luria Bertini broth, Mercuric chloride (95%), Mueller Hinton agar, Czapek dextrose agar, phosphate buffer solution (PBS), H_2O_2 (95%), NaCl (95%), and EDTA (95%), and Triton-X100 were purchased from Hi-media.

2.2. Preparation of Water hyacinth-mediated biogenic production of iron oxide nanoparticles

With some additional adaptations, we followed the protocol of (Periakaruppan et al. 2021) for the green synthesis of Fe-O-NP. Five grams of water hyacinth leaves were weighed. Thorough cleaning and washing were done under running water and again with double distilled water. Leaves were ground and 100 ml distilled water was added and boiled for 20–30 mins with constant stirring. After boiling the extract was filtered through Whatman No. 1 filter paper. The filter was then stored at 4°C in a sterile beaker for later use. After continuous stirring, 20 mL of water hyacinth leaf extract was added dropwise to 80 mL of aqueous ferrous sulfate heptahydrate ($Fe_2SO_4.7H_2O$) (0.1 M). NaOH was added to the mixture to obtain and then maintained a pH of 12. After centrifuging the precipitated liquid at 10,000 rpm for 30 minutes, impurities were removed by washing two or three times with Millipore water. To air dry the assortment, it was placed in a hot air oven at 120°C for 60 minutes. For further analysis and evaluation, the pellet was crushed and kept in a sterile container. (Fig. 1).

2.3. Material characterization

X-ray diffraction was used to study the crystallinity, phase purity, and crystallite size of Fe-O-NP. The hydrodynamic size of Fe-O-NP and their distribution pattern were measured using dynamic light scattering, with some modifications as described (Dhak et al. 2011). The UV-visible spectrum of Fe-O-NP synthesized by green methods was done using a Hitachi 330 spectrophotometer. Elemental composition of Fe-O-NP was done using energy-dispersive X-ray spectroscopy (EDS), while scanning electron microscopy (SEM) was used to study and record the surface morphology and approximate shape of the particles.

2.4. Antibacterial capacity of Fe-O-NPs against PGPR TIU16A3

The antibacterial activity of iron oxide nanoparticles prepared from *E. crassipes* extracts against TIU16A3 was evaluated by the agar well diffusion method. Zones of inhibition were evaluated to determine the degree of inhibition of bacterial growth.

2.5. Antifungal analysis of Fe-O-NPs on growth of *Fusarium* sp.

The antifungal activity of Fe-O-NP was analyzed with *Fusarium* sp., obtained from the Department of Plant Biology, Bose Institute, and Kolkata. Using Fe-O-NP, the fungal strain was inoculated onto Cazpek dextrose agar (CDA). Growth was examined on days three, six, and nine. Analysis was done based on colony diameter measurements using the formula for PIRG (percentage inhibition in radial growth) % = (R1– R2 ÷ R1) × 100 (Eq. 2), where R1 is the radial growth of the control and R2 is the radial growth of each treatment was used to determine the percentage of inhibition of fungal growth(Yazid et al. 2023).

2.6. Hemolytic analysis

The hemolysis assay typically uses fresh human blood samples from healthy adult volunteers stabilized with ethylenediaminetetraacetic acid (EDTA). With some modifications, the test was performed as previously mentioned (Modi et al. 2023). From serum, Red blood cells (RBC) were first separated by centrifugation at 2000 rpm for 10 min. After that, 5 ml of blood was added to 10 ml of 50 mM PBS. RBCs were then washed three more times using 50 mM PBS. A hematocrit of 5% was then used to dilute the purified erythrocytes in PBS. 100 µl of erythrocyte suspension was added to an eppendorf tube containing 100 µl of Fe-O-NPs at different concentrations (50, 100, 150, and 200 µg/mL). After one hour incubation at 37°C, centrifugation at 1500 rpm for ten minutes was done. The 80 µl supernatant was then added to PBS. Absorbance at 414 nm OD was measured using a plate reader. A positive control of 100% hemolysis was achieved using 0.1% Triton X-100 (v/v), while a negative control using PBS. The percentage of hemolysis was calculated using formula

% hemolysis = (OD of sample-OD of PBS) / (OD of positive control-OD of PBS) × 100 (Eq. 3)

2.7. Priming seeds of *Vigna radiata* L., germination, and transfer of seedlings in hydroponics culture

For seed priming, the seed of *Vigna radiata* L. (mung bean) procured from West Bengal State Seed Corporation Limited, Kolkata, West Bengal was used. Surface sterilization, priming with Fe-O-NP alone and synergistic with *Pseudomonas geniculata* TIU16A3, germination, and seedlings were transferred to a hydroponics solution for further experiments were done following the method(Kundu and Ganesan 2020, 2023a; Madhogaria et al. 2024a).

2.8. Standardization of Fe-O-NP for plant growth promotion

Treatments included control and different concentrations of Fe-O-NPs (25, 50, and 100 µg/mL) in three replicates were chosen for this analysis. Fe-O-NP treatment with maximum germination of *V. radiata* L. seedlings and maximum increment in different phenotypic plant traits (root length, shoot length, fresh weight. dry weight, secondary root number, secondary root length, leaves breadth, and leaves length)was selected for further experiment for analysis of heavy metal alleviation and plant growth promotion of *V. radaiata* L. in the presence of Cd, Cr, and Pb stress following the methods with some modifications by(Kundu and Ganesan 2023b).

2.9. Phenotypic differences between untreated, individually treated, and co-treated Vigna radiata L. plants and total biomass studies in the presence of heavy metal toxicity

The difference in plant growth was observed after 14 days of reading with the following treatments: untreated (UT), Fe-O-NP 50 µg/ml treated (T), TIU16A3 *P. geniculata* treated (T), and Fe-O-NP (50 µg/ml) + TIU16A3 treated plants in the presence and absence of heavy metals (chromium, cadmium, and lead) was done as described by(Madhogaria et al. 2024a). The traits analyzed for plant growth variation are primary root length, shoot length, dry weight, wet weight, leaf width, leaf length, total chlorophyll content, number of secondary roots, and secondary root length(Kundu and Ganesan 2023b).

2.10. Antioxidant SOD, POD, CAT, H_2O_2 content, and Electrolyte leakage (EL) analysis

Determination SOD, POD, CAT, H_2O_2, and electrolyte leakage estimation was done as described by (Madhogaria et al. 2024a) with some modifications.

2.11. Determination of HMs (Cr, Cd, and Pb) content

A 3:1 mixture of sulfuric and nitric acid was used to digest 100 mg of dry plant material. Further analysis was done as described by **(**Madhogaria et al. 2024a) with some modifications.

2.12. Analysis of gene expression by RT-qPCR

The transcript levels of gene *Aux/IAA* of shoot tissue of *Vigna radiata* L. plant in the presence of 10, and 20 µg/mL of HMs Cr, and Cd stress with Fe-O-NP alone and *P. geniculata* + 50µg/mL Fe-O-NPs were determined by real-time PCR following the method with some medication by (Madhogaria et al. 2024a).

2.13. Statistical analysis

All the tests were performed in triplicates to avoid any errors and to increase the accuracy. All graphical analyses were performed using Graph pad prism 8.0.2 and Origin Pro 8.5.0. Statistical significance differences among different treatments were done using Duncan's multiple range test (DMRT) using software IBM SPSS version 16. Statistical probability $P < 0.05$ was followed.

3. Results and Discussions

3.1. Material characterization

3.1.1. UV-visible spectroscopy

UV–Vis absorption spectrum showed a wide absorption peak at 595 nm. The firm transmission peaks were observed at 568nm with 84.54% transmission, 588nm with 89.8% transmission, 595nm with 91.38% transmission, and 629nm with 91.51% transmission. Figure 2 depicts the transmission spectra of *E.crassipes* mediated biogenic synthesis of Fe-O-NPs falls between 400–700 nm. According to (Basavegowda et al. 2014) using *A. annua* and *P. frutescens* green synthesized iron oxide NP had a similar range by which we can confirm that metal-oxide nanoparticles are being formed.

3.1.2. X-ray diffraction analysis

The X-ray diffraction (XRD) patterns were analyzed with the JCPDS card file 19–0629 89–0596, confirming the formation of amorphous magnetite iron oxide nanoparticles. The scanning speed is 10^0/min. The amorphous nature and composition of Fe-O-NP were evaluated over a 2θ range from 30^o to 70^o (Fig. 3). The diffraction peaks were present at 35° (104), 42° (113), 52° (018), and 64° (024). The average crystallite size of Fe-O-NP was 15.5 nm, calculated using the Scherrer equation. The intensity of diffraction peaks signifies good crystallinity of the synthesized nanoparticles. Moreover, similar results have been reported by (Yew et al. 2017; Yadav et al. 2020).

3.1.3. Dynamic light scattering analysis

The intensity-average diameter of Fe-O-NP was calculated at 1026 nm by using dynamic light scattering (DLS) analysis. The hydrodynamic size distribution of Fe-O-NP is shown in (Fig. 4). It is the core size and the presence of capping elements around it. NPs were at moderate stability and exhibited excellent dispersion in an aqueous medium.

3.1.4. Scanning electron microscopy wit henergy-dispersive X-ray mapping

Structural analysis of biogenic Fe-O-NP can be done precisely by scanning electron microscopy (SEM). Fe-O-NPs surface morphology and elemental composition are illustrated in (Fig. 5). As obtained by using SEM analysis, respectively. Energy dispersive X-ray (EDX) analysis reported the presence of 32.62% iron

and 34.97% oxygen along with 31.88% carbon due to the availability of phyto-phenolic compounds in Fe-O-NP synthesized from *E. crassipes* (Fig. 6). Similar results were reported by (Periakaruppan et al. 2021).

3.2. Antibacterial evaluation

Minimum inhibitory concentration MIC is evaluated for our synthesized Fe-O-NP against TIU16A3 (accession no. OR507186). We observed that Green synthesized Fe-O-NP has no antibacterial effect against TIU16A3 as no zone of inhibition was formed (Fig. 7). We can imply from this result that the green synthesized Fe-O-NPs from *E. crassipes* andTIU16A3can be used in combination on the seed of *V. radiata* L.to study synergistic effect on heavy metal mitigation and plant growth promotion.

3.3. Antifungal evaluation

Biogenic Fe-O-NP synthesized in this study revealed remarkable antifungal potency against *Fusarium* sp. when compared to the control Fig. 8. Radial growth size of fungus in the presence of 25, 50, and 100µg/mL was measured to be 25mm, 16mm, and 17mm respectively. Percent inhibition of radial growth (PIRG) was calculated with the help of Eq. 2 and PIRG% for 25 µg/mL was 44.4%, similarly for 50 µg/mL, the PIRG% was 64.4%, and for 100 µg/mL 62.2% was the PIRG%. This result suggested that as the concentration of Fe-O-NP is increasing, inhibition of the fungus growth is also increasing. The gradual increment of the inhibition potential rate of green-synthesized Fe-O-NPs may be due to their high effect on the growth of fungal mycelium. The biogenic Fe-O-NPs synthesized from the leaf extract of *Euphorbia herita* showed excellent antifungal activity against *Aspergillusniger*, *Arthogrophis cuboida*, and *Aspergillus fumigatus* in the range of 10–30 mg/mL (Win et al. 2021). Another study confirmed the potential antifungal activity of Fe-O-NPs synthesized from *Chlorella*-K01 extract against *Fusarium oxysporum*, *Fusarium tricinctum*, and *Fusarium maniliforme* (Cruz-Luna et al. 2023). Thus, the present findings and previous reports signify the efficiency of biogenic Fe-O-NPs usage as potent natural fungicides in comparison with chemical-toxic fungicides. In addition, the application of biologically synthesized Fe-O-NPs affirms fungal resilience resulting from the extensive use of chemical fungicides. The interaction of NPs with fungal cells might lead to the elimination of cytoplasmic membranes (Ahmed et al. 2021). The disruption of the fungal cell membrane is attributed to the secretion of micro-ions such as potassium and phosphate radicals, along with large-sized molecules such as RNA, DNA, and other intracellular substances (Ojoma et al. 2021).

3.4. Hemolytic activity

The hemolytic effect of biogenic Iron oxide NP was carried out by Human RBC hemolytic assay in the presence of different Fe-O-NP concentrations (Fig. 9). At concentrations of 50, 100, 150, and 200 µg/mL of biogenic Fe-O-NP, the hemolysis level was below 15% even at the highest concentration (200 µg/mL) in comparison of the value of 0.1% Triton X100 (positive control) mediated hemolysis. The reason behind the non-toxic behavior against human RBC of our green synthesized is that it has been previously studied that biogenic Fe-O-NPs are biocompatible, biodegradable, and potentially nontoxic to humans (Wahajuddin and Arora 2012).

3.5. Standardization of different concentrations of biogenic Fe-O-NP for the promotion of plant growth

Fe-O-NP effect on seedling growth and different growth parameters, in *V. radiata* L. plants, to understand its mode of action and to establish an optimal concentration for plant growth promotion. We used 25, 50, and 100 µg/mL for the test. Seed priming was done, Non-primed seeds were kept as control. We found out that seed germination was highest at 50 µg/mL of Fe-O-NP concentration at which root length was 65.2 mm in length when compared to control 23.5 mm (Fig. 10) Analysis of different phenotypic plant traits was done and we found out that at 50 µg/mL of Fe-O-NP concentration, shoot length increased up to 38% in comparison to 25 and 100 µg/mL. The secondary root number and its length showed more growth in 50µg/mL of Fe-O-NP concentration (Fig. 11). Similar results were seen in the case of the length and breadth of leaves. If we cumulatively analyze the growth in all the plant traits in different concentrations we can say that growth was 54.4% higher in 50 µg/mL than in 25, and 100 µg/mL of Fe-O-NP treated plants. Fe-O-NPs release iron. Iron affects plant metabolism, photosynthesis, and respiration. Electron carriers like cytochromes, ferredoxins, etc. are being affected by iron (Hochmuth 2011). The vigorous growth of *V. radiata* L. plants under the effect of Fe-O-NPs is because of enhancement in auxin, metabolism enhancement, cell expansions, and enhanced biochemical activities which ultimately lead to growth in various morpho-physiological traits of the plant. Similar results were reported by (Iqbal et al. 2019)

3.6. Effect of green synthesized Fe-O-NPs 50µg/mL on V. radiata L. growth and photosynthetic content under heavy metal stress

The seedlings exposed to Fe-O-NP (50 µg/mL) exhibits increased nutrient uptake, followed by stimulation of plant growth, and improvement of morphological and physiological characteristics of *V. radiata* L. seedlings (Fig. 12). Compared with control and NP-treated seedlings, heavy metal treatment negatively affected the growth of *V. radiata* L. seedlings. Compared to HM treated seedlings, Fe-O-NP treated seedlings showed better root length (54.2%) and shoot length (62.8%) difference ($P \leq 0.05$) (Fig. 13a), (Fig. 13b). *V. radiata* L. seedlings treated with Fe-O-NPs showed a significant ($P \leq 0.05$) increase in both fresh and dry weight compared to the control group (Fig. 13c) (Fig. 13d).The root length increased up to 73%, and 67%and shoot length 75%, and 71% for Cr and Cd HM stress in presence of Fe-O-NP. A negligible growth range from 21.4–31% increment was observed in lead stress for Fe-O-NP 50 µg/mL treatment. Fresh weight and dry weight of the Fe-O-NP treated test crop were increased 79% and 85.2% respectively in the presence of 10 µg/mL of Cr to control followed by increase in fresh and dry weight of Fe-O-NP treated *V. radiata* L. in the presence of Cd 10 µg/mL which was 65.4% and 69.7% respectively. At 20 µg/mL of Cr and Cd fresh and dry weight were observed in the range of (61.4–63.7%) fresh weigh and dry weight respectively. In presence of lead in all concentrations Fe-O-NP treated *V. radiata* L. exhibited minimal growth in fresh and dry weight ranging from 24–31%. Which is less than the Fe-O-NP treated *V. radiata* L. growth observed in Cr and Cd stress in 10 and 20 µg/mL concentrations. A similar pattern was observed in leaf length, breadth, and chlorophyll content in Fe-O-NP-treated *V. radiata*

L. in the presence of different concentrations of Cr, Cd, and Pb. At 10 and 20 µg/mL of Cr and Cd increase in leaf breadth was prominent with 24.3–24.1% was no prominent difference in leaf breadth and length was observed in other concentrations (Fig. 13e) (Fig. 13f) (Fig. 13g).Thus we can say that the best variations in phenotypic traits root length, shoot length, fresh and dry weight, leaf length, leaves breadth, and photosynthetic pigment were observed in Fe-O-NP treated *V. radiata* L. in Cr and Cd at 10 µg/mL and 20 µg/mL of stress.

Roots appear to transport green synthesized Fe-O-NPs into plant tissues when they are treated with the synthesized nanoparticles and grown in Hoagland's solution. The increased uptake of potassium, phosphorus, and nitrogen in the presence of iron is thought to be the main reason for the increase in growth and total biomass of plants treated with Fe-O-NP. Fe-O-NP also works against the negative effects of sodium and chloride ions (Tawfik et al. 2021). According to reports, cadmium accumulation in crops decreased when the concentration of Fe-O-NPs increased (Sebastian et al. 2017; Rizwan et al. 2019). Similarly, Fe and Fe_3O_4 NPs were found to be more effective than other methods in reducing arsenic (As) in rice plants (Lux et al. 2011; Huang et al. 2020), have reported that cadmium and iron have the same transport pathways during their uptake in plants, and under the situation of iron deficiency, iron transporters are activated, reducing the cadmium uptake and accumulation in crop plants. (Bashir et al. 2018) have suggested that due to competitive adsorption, the accumulation of heavy metals like cadmium is reduced in the presence of higher concentrations of iron.

3.7. Effect of Fe-O-NPs 50µg/mL and TIU16A3 on V. radiata L. growth and photosynthetic content under heavy metal stress

In that study, different concentrations of Cr, Cd, and Pb (i.e. 0 µg/mL, 10 µg/mL, 20 µg/mL, 40 µg/mL, and 80 µg/mL) were used to grow *V. radiata* L. seedlings. In addition, TIU16A3, seeds were treated with 50 µg/mL green synthesized Fe-O-NP. Figures 12 and 13 show information on shoot length, root length, fresh weight, dry weight, secondary root length, and number. Figure 14 shows the data on the length and width of the leaves and the total chlorophyll content. The findings showed that, in *V. radiata* L. seedlings in the presence of rising levels of Cr, and Cd considerably reduced biomass when compared to plants grown with the application of TIU16A3 and Fe-O-NP, the application of these two substances to the seeds of *V. radiata* L resulted in a significant increase in shoot length, root length, fresh weight, dry weight, secondary root length, leaves length, breadth, and content of total chlorophyll of Cr, Cd and Pb stress. The Fe-O-NP with PGPB (*P. geniculata*) had the best effect on Cr and Cd (10 µg/mL, 20 µg/mL), followed by 40 µg/mL and 80 µg/mL, according to our results. Pb exhibited growth but was least effective which is why our further studies were focused on the effective HM concentrations.

There is a direct correlation between plant growth and biomass, which increased up to 90.89% more after the augmentation of TIU16A3 and 50 µg/ml Fe-O-NP in combination under heavy metal toxicity. Total chlorophyll contents were 69% and 63% respectively in the presence of Fe-O-NP alone, but the increment was 83% in combination as depicted in Fig. 15.Fe-O-NP 50µg/mL + TIU16A3 exhibited a synergistic effect on root growth under heavy metal Cr, and Cd stress and the effectiveness of combined

treatment was maximum in Cr 84.6%, followed by Cd 92% as illustrated in Fig. 12. This is maximum growth compared to TIU16A3 treatment and Fe-O-NP 50µg/mL. Thus, we can say that the combinatorial effect is best for *V. radiata* L. growth in the presence of Cr and Cd strain is most effective at lower concentrations of Cd and Cr. This exponential increase in the phenotypic traits of *V. radiata* L. in the presence of TIU16A3 and Fe-O-NP 50 µg/mL together than individually could be due to the acceleration in the accumulation of mineral nutrients from NPs.

Compared to the use of PGPR or NP alone, the combined use of both can improve crop productivity, plant height, dry-fresh biomass, and seed germination frequency (Medina-Velo et al. 2017). This combination can work in many different ways. Improved plant performance and productivity result from direct mechanisms including PGPR, regular production of plant hormones (e.g., indoleacetic acid, siderophores, etc.), and increased soil mineral availability through phosphate solubilization and N_2 fixation. The presence of NPs can help PGPR tolerate higher density while providing a nutrient-rich substrate that improves PGPR efficiency and increases plant production (Rani et al. 2008; Mushtaq et al. 2020). In the presence of heavy metal contamination by exploiting the ability of PGPR to release exopolysaccharides under dry conditions, plants can increase their stress tolerance (Bishnoi Saran 2015; Vurukonda et al. 2016).

3.8. Effect of 50 µg/mL Fe-O-NPs and TIU16A3 on superoxide dismutase (SOD), peroxidase (POD), and catalase (CAT), H_2O_2 content, and electrolyte leakage (EL) in Vigna radiata L. under heavy metal stress

Cd and Cr stress significantly increased H_2O_2 content and EL value; however, when treatment of 50 µg/mL Fe-O-NP and TIU16A3 were given on *Vigna radiata* L. the leakage percentages of H_2O_2 and EL of the respective controls were reduced by 37.5% and 43% and 21.5% and 26%, respectively (Fig. 15d), and (Fig. 15e). Activities of invertase and catalase in soil were significantly higher when *P. geniculata* was used with NPs than when NPs were used alone (Khanna et al. 2021). In summary, the results show that PGPR with NPs increases the enzymatic activity of sucrose, urease, protease, and invertase in addition to soil phosphomonoesterase under both acidic and basic conditions. There is a direct correlation between soil nutrients and the enhanced enzyme activity of antioxidant-responsive genes caused by PGPR and NPs (Mushtaq et al. 2020).

3.9. Effect of 50µg/mL Fe-O-NPs and TIU16A3 on metal uptake by plant *Vigna radiata* L.

By Flame Atomic Absorption Spectroscopy (FAAS) analysis of the total metal contents and the accumulation was done. The results show that the plant tissues accumulate more Cr and Cd (10 µg/mL, and 20 µg/mL) in non-inoculated plants in comparison to 50 µg/ml Fe-O-NP and TIU16A3inoculated. FAAS data of Cr and Cd metals in the presence of synergistic treatment of 50 µg/mL Fe-O-NP and TIU16A3 showed that there was a reduction in metal content by30.6% in comparison to individual treatment as depicted in (Fig. 16a), and (Fig. 16b).

Fe-O-NP and TIU16A3 combined increased soil enzyme (dehydrogenase) more than NPs, and *P. geniculata* alone which must have resulted in better biological remediation. Previous studies have shown that the combined use of PGPR and NP decreased Cd levels more effectively than the use of NP and PGPR alone. TIU16A3 and NPs together reduced significantly the harmful effects of chromium and promoted plant growth. This may be because PGPRs and NPs limit the availability of metals for uptake and translocation in soil (Mitra et al. 2018).

3.10. Effect of 50µg/mL Fe-O-NPs andTIU16A3 synergistically on gene expression of Aux/IAA of shoot tissue in V. radiata L. under heavy metal stress

In the present study, gene expression profiling of auxin-responsive genes in seedlings under Cr and Cd metal stress has been studied through qRT-PCR which exhibits a high expression of the gene of interest in the presence of 50 µg/mL Fe-O-NPs and TIU16A3 together as shown in Fig. 17.

4. Conclusion

This study aimed to determine whether *Eichhornia crassepis* plant extract and green synthesized iron oxide nanoparticles (Fe-O-NP) could protect Moong bean plants against heavy metal stress. The deleterious effects of metal stress on plants were confirmed by significantly increased electrolyte leakage and hydrogen peroxide (H_2O_2) levels. Increases in biomass, photosynthetic pigments, nutrients, and indole acetic acid in plants treated with Fe-O-NP and PGPR and exposed to all concentrations of heavy metal stressors, all of which improved plant growth. Reduction of heavy metals by treatment is associated with improved plant growth based on Flame Atomic Absorption Spectrophotometry. TIU16A3 and Fe-O-NPs work together to reduce antioxidant enzymes, mainly catalase, peroxidase, and superoxide dismutase, which signifies that the synergistic treatment reduced the stressed condition in the plant. In addition, significant reductions in electrolyte leakage and H_2O_2 indicated that this treatment alleviated heavy metal stress. The results of this study indicated that plants can be protected against single and combined heavy metal stress caused by Cr, and Cd through the complementary effects of PGPR and Fe-O-NPs. Therefore, Fe-O-NPs are suitable for agricultural applications in living organisms instead of chemically synthesized Fe-O-NPs due to their negligible side effects. Eco-friendly production and development of super-stabilized nanoparticles is promising because it uses few harmful chemicals and high energy consumption. In addition to enhancing plant tolerance, the interaction of PGPR and Fe-O-NPs opens the door to long-term increases in yield. By combining the strengths of these two factors, we can open new opportunities to improve plant health and productivity, an important step forward in the search for sustainable agricultural methods.

Declarations

Acknowledgment

The authors thank Techno India University, West Bengal for their encouragement and support during this study.

Author's contribution

P.D. and A.K. designed and conceptualized the experiment. B.M. performed the experiments, synthesis and material characterization, data analysis, and paper writing. S.B. performed the synthesis and material characterization of the sample, data analysis, and paper writing. S.C. helped in editing. All authors have checked the current form of this manuscript.

Data availability

This article incorporates all the data examined during this research.

Compliance with ethical standards

Ethics statement

This study did not involve any human or animal participants to conduct the research work.

Informed consent

No patient data were reported.

Competing interests

The authors have no competing interests to declare that are relevant to the content of this article.

Funding

The authors did not receive support from any organization for the submitted work.

References

1. Ahmed B, Rizvi A, Syed A, et al (2021) Differential responses of maize (*Zea mays*) at the physiological, biomolecular, and nutrient levels when cultivated in the presence of nano or bulk ZnO or CuO or Zn2+ or Cu2+ ions. Journal of Hazardous Materials 419:126493. https://doi.org/10.1016/j.jhazmat.2021.126493
2. Banerjee S, Kundu A, Dhak P (2022) Bioremediation of uranium from waste effluents using novel biosorbents: a review. J Radioanal Nucl Chem 331:2409–2435. https://doi.org/10.1007/s10967-022-08304-2
3. Banerjee S, Mukherjee A, Kundu A (2023) The current scenario and future perspectives of transgenic oilseed mustard by CRISPR-Cas9. Mol Biol Rep 50:7705–7728. https://doi.org/10.1007/s11033-023-08660-6

4. Basavegowda N, Magar KBS, Mishra K, Lee YR (2014) Green fabrication of ferromagnetic Fe3O4 nanoparticles and their novel catalytic applications for the synthesis of biologically interesting benzoxazinone and benzthioxazinone derivatives. New J Chem 38:5415–5420. https://doi.org/10.1039/C4NJ01155D
5. Bashir A, Rizwan M, Ali S, et al (2018) Effect of foliar-applied iron complexed with lysine on growth and cadmium (Cd) uptake in rice under Cd stress. Environ Sci Pollut Res Int 25:20691–20699. https://doi.org/10.1007/s11356-018-2042-y
6. Bishnoi Saran U (2015) PGPR Interaction: An Ecofriendly Approach Promoting the Sustainable Agriculture System. In: Advances in Botanical Research. p 33 (81-113)
7. Cruz-Luna A, Vásquez-López A, Rojas-Chávez H, et al (2023) Engineered Metal Oxide Nanoparticles as Fungicides for Plant Disease Control. Plants 12:. https://doi.org/10.3390/plants12132461
8. Dhak P, Dhak D, Das M, Pramanik P (2011) Dielectric and impedance spectroscopy study of Ba0.8Bi2.133Nb1.6Ta0.4O9 ferroelectric ceramics, prepared by chemical route. J Mater Sci: Mater Electron 22:1750–1760. https://doi.org/10.1007/s10854-011-0358-1
9. Gupta A, Sinha S, Basant A, Singh K (2007) Multivariate Analysis of Selected Metals in Agricultural Soil Receiving UASB Treated Tannery Effluent at Jajmau, Kanpur (India). Bulletin of environmental contamination and toxicology 79:577–82. https://doi.org/10.1007/s00128-007-9287-3
10. Hochmuth G (2011) Iron (Fe) Nutrition of Plants. EDIS 2011:. https://doi.org/10.32473/edis-ss555-2011
11. Huang X, Wu S, Tang S, et al (2020) Photocatalytic hydrogel layer supported on alkali modified straw fibers for ciprofloxacin removal from water. Journal of Molecular Liquids 317:113961. https://doi.org/10.1016/j.molliq.2020.113961
12. Iqbal J, Abbasi B, Ahmad R, et al (2019) Biogenic synthesis of green and cost effective iron nanoparticles and evaluation of their potential biomedical properties. Journal of Molecular Structure 1199:. https://doi.org/10.1016/j.molstruc.2019.126979
13. Khanna K, Kohli SK, Handa N, et al (2021) Enthralling the impact of engineered nanoparticles on soil microbiome: A concentric approach towards environmental risks and cogitation. Ecotoxicol Environ Saf 222:112459. https://doi.org/10.1016/j.ecoenv.2021.112459
14. Kiwumulo HF, Muwonge H, Ibingira C, et al (2022) Green synthesis and characterization of iron-oxide nanoparticles using Moringa oleifera: a potential protocol for use in low and middle income countries. BMC Research Notes 15:149. https://doi.org/10.1186/s13104-022-06039-7
15. Kundu A, Das S, Basu S, et al (2019) GhSTOP1, a C2H2 type zinc finger transcription factor is essential for aluminum and proton stress tolerance and lateral root initiation in cotton. Plant Biol (Stuttg) 21:35–44. https://doi.org/10.1111/plb.12895
16. Kundu A, Ganesan M (2020) *GhMATE1* expression regulates Aluminum tolerance of cotton and overexpression of *GhMATE1* enhances acid soil tolerance of Arabidopsis. Current Plant Biology 24:100160. https://doi.org/10.1016/j.cpb.2020.100160

17. Kundu A, Ganesan M (2023a) Low pH stress activates several genes for lateral root formation and detoxification of Aluminum ions in cotton plants. Plant Stress 9:100188. https://doi.org/10.1016/j.stress.2023.100188
18. Kundu A, Ganesan M (2023b) Al Stress Activates Several Genes for Lateral Root Formation and Al Detoxification in Cotton Seedlings
19. Lux A, Martinka M, Vaculík M, White PJ (2011) Root responses to cadmium in the rhizosphere: a review. J Exp Bot 62:21–37. https://doi.org/10.1093/jxb/erq281
20. Madhogaria B, Banerjee S, Chakraborty S, et al (2024a) Alleviation of heavy metals chromium, cadmium and lead and plant growth promotion in Vigna radiata L. plant using isolated Pseudomonas geniculata. International Microbiology 1–17. https://doi.org/10.1007/s10123-024-00546-2
21. Madhogaria B, Banerjee S, Kundu A, Dhak P (2024b) Efficacy of new generation biosorbents for the sustainable treatment of antibiotic residues and antibiotic resistance genes from polluted waste effluent. Infectious Medicine 3:100092. https://doi.org/10.1016/j.imj.2024.100092
22. Madhogaria B, Bhowmik P, Kundu A (2022) Correlation between human gut microbiome and diseases. Infectious Medicine 1:180–191. https://doi.org/10.1016/j.imj.2022.08.004
23. Medina-Velo IA, Barrios AC, Zuverza-Mena N, et al (2017) Comparison of the effects of commercial coated and uncoated ZnO nanomaterials and Zn compounds in kidney bean (Phaseolus vulgaris) plants. J Hazard Mater 332:214–222. https://doi.org/10.1016/j.jhazmat.2017.03.008
24. Mitra S, Pramanik K, Sarkar A, et al (2018) Bioaccumulation of cadmium by Enterobacter sp. and enhancement of rice seedling growth under cadmium stress. Ecotoxicol Environ Saf 156:183–196. https://doi.org/10.1016/j.ecoenv.2018.03.001
25. Mondal T, Datta JK, Mondal NK (2017) Chemical fertilizer in conjunction with biofertilizer and vermicompost induced changes in morpho-physiological and bio-chemical traits of mustard crop. Journal of the Saudi Society of Agricultural Sciences 16:135–144. https://doi.org/10.1016/j.jssas.2015.05.001
26. Mushtaq T, Shah AA, Akram W, Yasin NA (2020) Synergistic ameliorative effect of iron oxide nanoparticles and Bacillus subtilis S4 against arsenic toxicity in Cucurbita moschata: polyamines, antioxidants, and physiochemical studies. Int J Phytoremediation 22:1408–1419. https://doi.org/10.1080/15226514.2020.1781052
27. Nayana AR, Joseph BJ, Jose A, Radhakrishnan EK (2020) Nanotechnological Advances with PGPR Applications. In: Hayat S, Pichtel J, Faizan M, Fariduddin Q (eds) Sustainable Agriculture Reviews 41: Nanotechnology for Plant Growth and Development. Springer International Publishing, Cham, pp 163–180
28. Naz H, Naz A, Ashraf S (2015) Impact of Heavy Metal Toxicity to Plant Growth and Nodulation in Chickpea Grown Under Heavy Metal Stress. INTERNATIONAL JOURNAL FOR RESEARCH IN EMERGING SCIENCE AND TECHNOLOGY

29. Ojoma AQ, Davidb O, Chukwumad AC, et al (2021) TRANSMISSION DYNAMICS OF EBOLA VIRUS DISEASE WITH VACCINE, CONDOM USE, QUARANTINE, ISOLATION AND TREATMENT DRUG. Afr J Infect Dis 15:10–23. https://doi.org/10.21010/ajid.v15i1.2
30. Periakaruppan R, Chen X, Thangaraj K, et al (2021) Utilization of tea resources with the production of superparamagnetic biogenic iron oxide nanoparticles and an assessment of their antioxidant activities. Journal of Cleaner Production 278:123962. https://doi.org/10.1016/j.jclepro.2020.123962
31. Rani A, Shouche YS, Goel R (2008) Declination of copper toxicity in pigeon pea and soil system by growth-promoting Proteus vulgaris KNP3 strain. Curr Microbiol 57:78–82. https://doi.org/10.1007/s00284-008-9156-2
32. Rastogi A, Tripathi DK, Yadav S, et al (2019) Application of silicon nanoparticles in agriculture. 3 Biotech 9:90. https://doi.org/10.1007/s13205-019-1626-7
33. Rizwan M, Ali S, Ali B, et al (2019) Zinc and iron oxide nanoparticles improved the plant growth and reduced the oxidative stress and cadmium concentration in wheat. Chemosphere 214:269–277. https://doi.org/10.1016/j.chemosphere.2018.09.120
34. Saravanabhavan G, Werry K, Walker M, et al (2017) Human biomonitoring reference values for metals and trace elements in blood and urine derived from the Canadian Health Measures Survey 2007–2013. International Journal of Hygiene and Environmental Health 220:189–200. https://doi.org/10.1016/j.ijheh.2016.10.006
35. Sebastian A, Nangia A, Prasad MNV (2017) Carbon-Bound Iron Oxide Nanoparticles Prevent Calcium-Induced Iron Deficiency in Oryza sativa L. J Agric Food Chem 65:557–564. https://doi.org/10.1021/acs.jafc.6b04634
36. Tawfik M, Mohamed H, Sadak M, Thalooth A (2021) Iron oxide nanoparticles effect on growth, physiological traits and nutritional contents of Moringa oleifera grown in saline environment. Bulletin of the National Research Centre 45:. https://doi.org/10.1186/s42269-021-00624-9
37. Vurukonda SSKP, Vardharajula S, Shrivastava M, SkZ A (2016) Enhancement of drought stress tolerance in crops by plant growth promoting rhizobacteria. Microbiol Res 184:13–24. https://doi.org/10.1016/j.micres.2015.12.003
38. Wahajuddin, Arora S (2012) Superparamagnetic iron oxide nanoparticles: magnetic nanoplatforms as drug carriers. International Journal of Nanomedicine 7:3445–3471. https://doi.org/10.2147/IJN.S30320
39. Win EP, Win KK, Bellingrath-Kimura SD, Oo AZ (2021) Influence of rice varieties, organic manure and water management on greenhouse gas emissions from paddy rice soils. PLOS ONE 16:e0253755. https://doi.org/10.1371/journal.pone.0253755
40. Yadav V, Ali D, Khan S, et al (2020) Synthesis and Characterization of Amorphous Iron Oxide Nanoparticles by the Sonochemical Method and Their Application for the Remediation of Heavy Metals from Wastewater. Nanomaterials 10:1551. https://doi.org/10.3390/nano10081551
41. Yang X, Alidoust D, Wang C (2020) Effects of iron oxide nanoparticles on the mineral composition and growth of soybean (Glycine max L.) plants. Acta Physiol Plant 42:128.

https://doi.org/10.1007/s11738-020-03104-1

42. Yazid SNE, Tajudin NI, Razman NAA, et al (2023) Mycotoxigenic fungal growth inhibition and multi-mycotoxin reduction of potential biological control agents indigenous to grain maize. Mycotoxin Res 39:177–192. https://doi.org/10.1007/s12550-023-00484-4
43. Yew YP, Kamyar S, Miyake M, et al (2017) An Eco-Friendly Means of Biosynthesis of Superparamagnetic Magnetite Nanoparticles via Marine Polymer. IEEE Transactions on Nanotechnology PP:1–1. https://doi.org/10.1109/TNANO.2017.2747088
44. Zulfiqar U, Yasmin A, Fariq A (2022) Metabolites produced by inoculated Vigna radiata during bacterial assisted phytoremediation of Pb, Ni and Cr polluted soil. PLoS One 17:e0277101. https://doi.org/10.1371/journal.pone.0277101

Figures

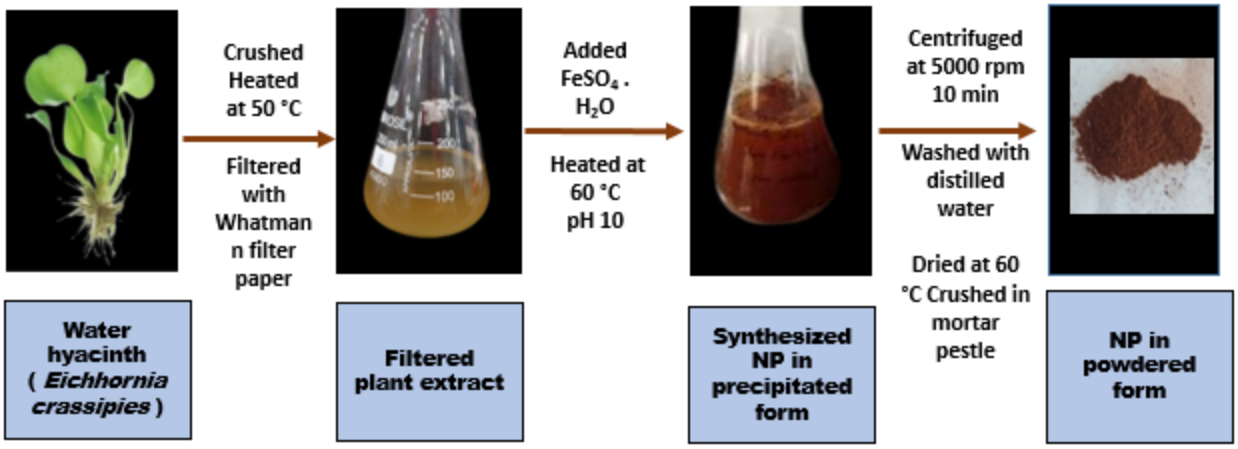


Figure 1

Flow diagram for the synthesis of desired Fe-O-NP from water hyacinth plant extract

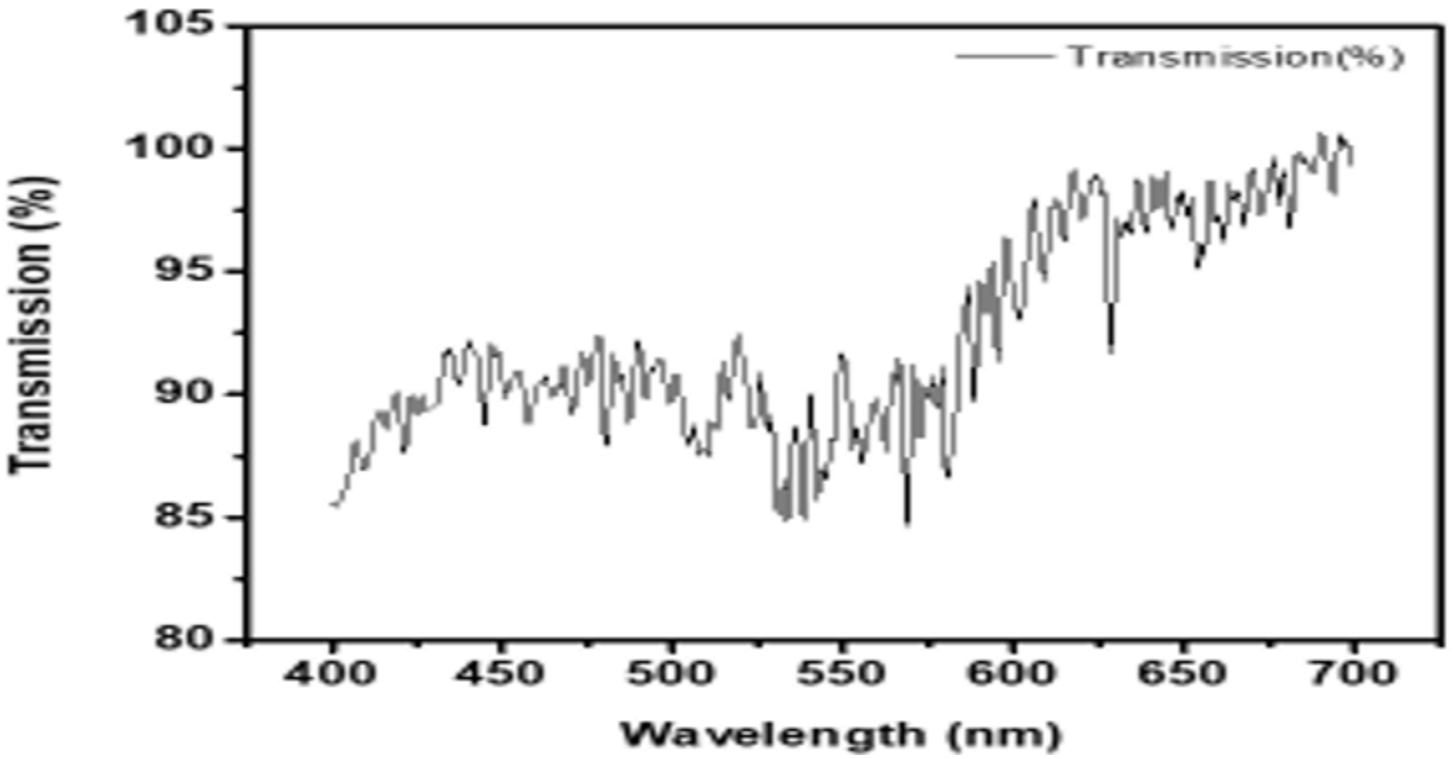


Figure 2

UV-visible absorption spectra of biogenic iron oxide nanoparticles from Water Hyacinth

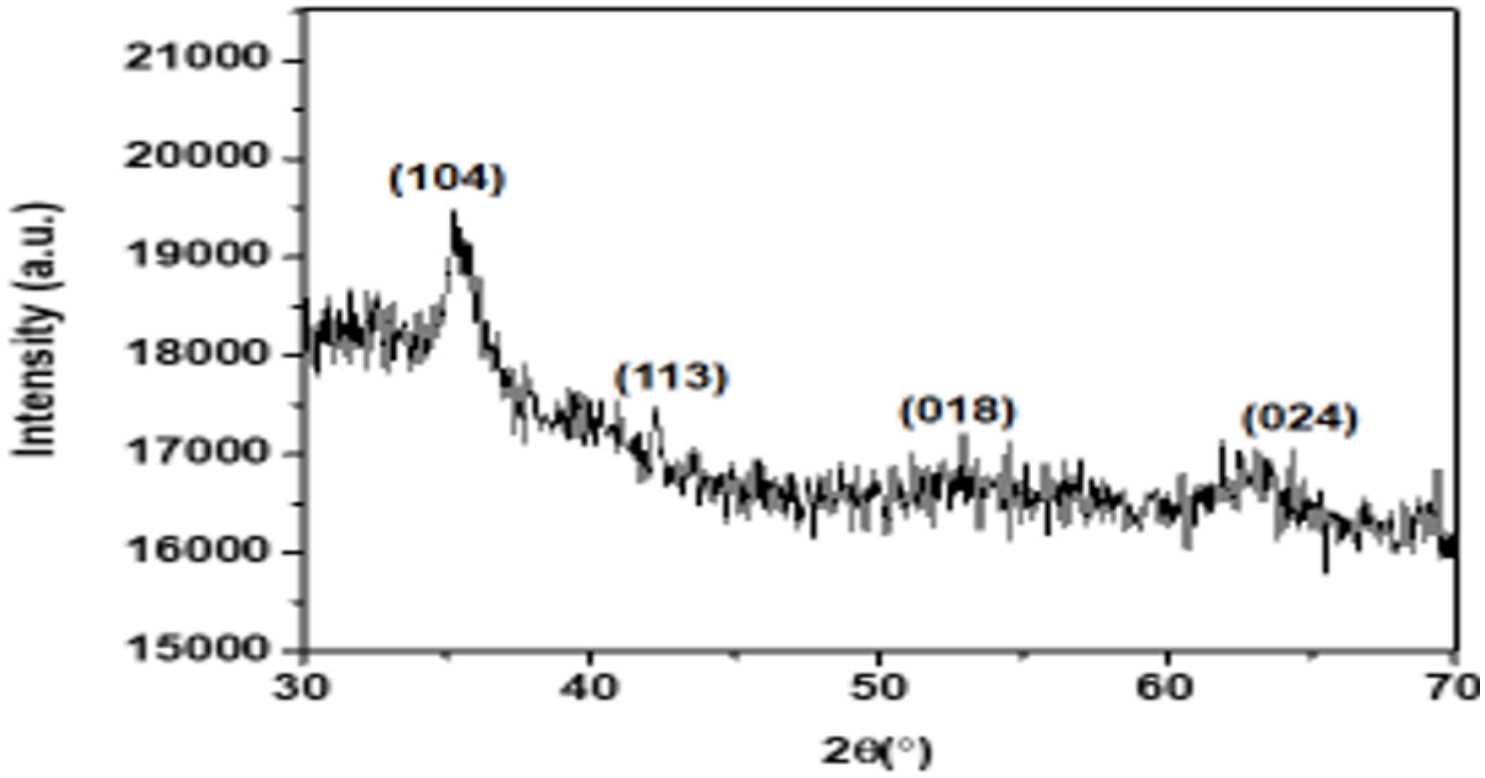


Figure 3

XRD diffraction pattern of biogenically synthesized iron oxide nanoparticles from water hyacinth

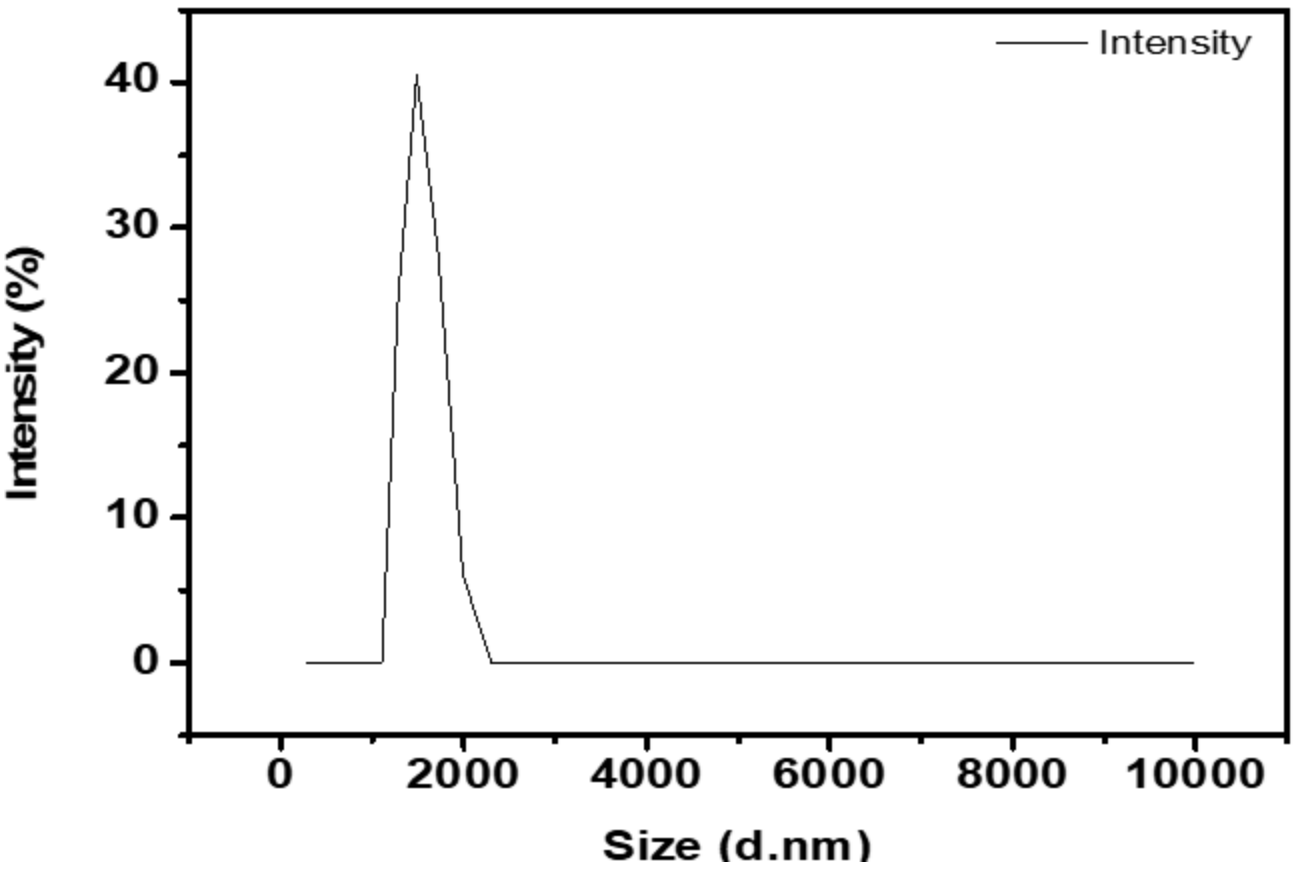


Figure 4

DLS analysis of biogenically synthesized iron oxide nanoparticles from water hyacinth

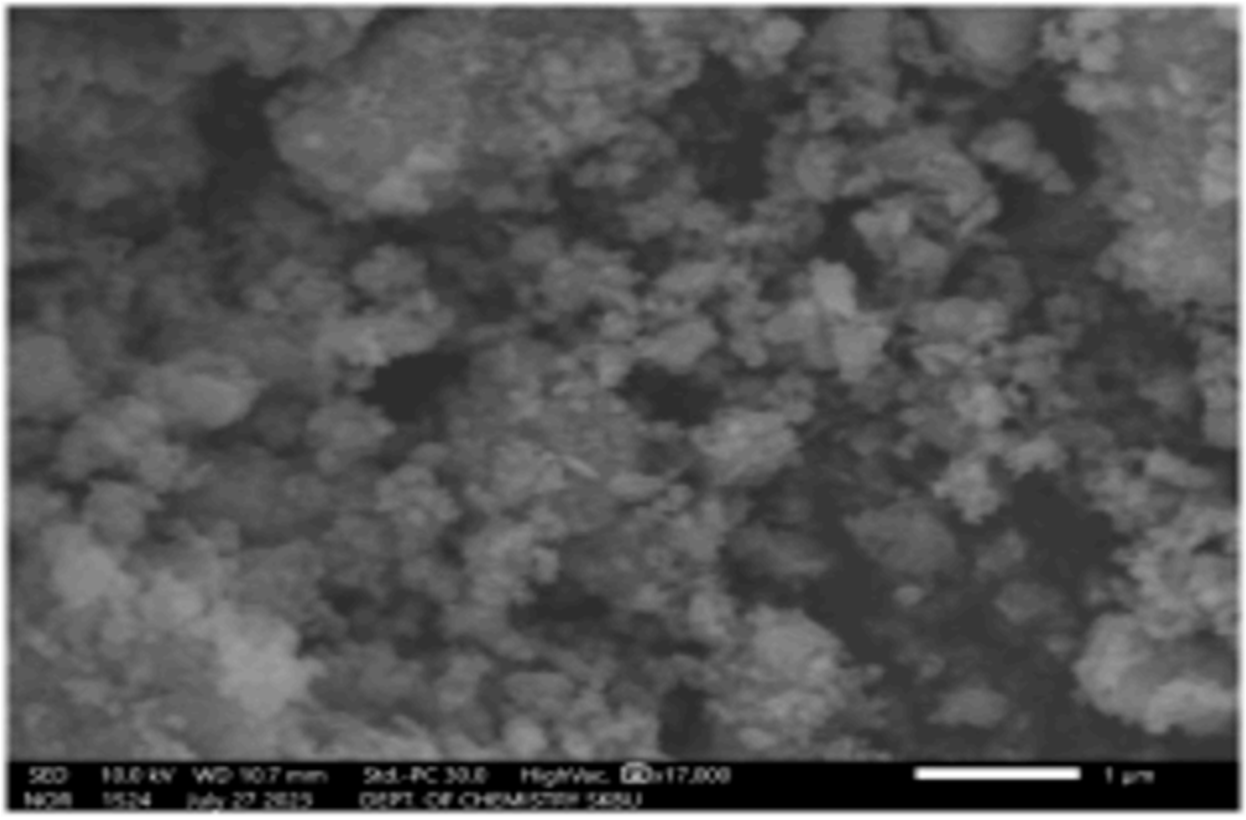


Figure 5

SEM image of biogenically synthesized iron oxide nanoparticles from water hyacinth

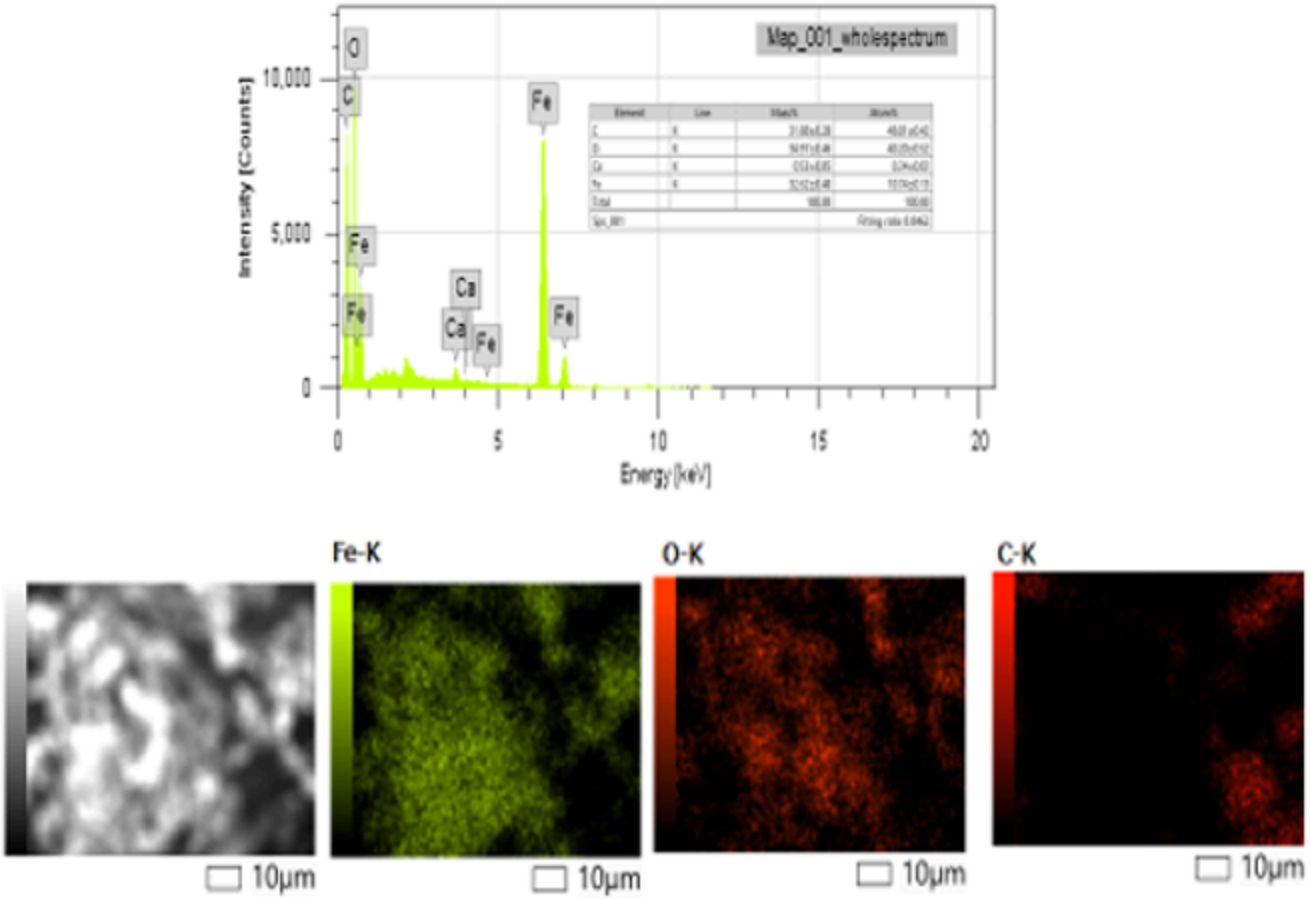


Figure 6

EDX analysis of biogenically synthesized iron oxide nanoparticles from water hyacinth

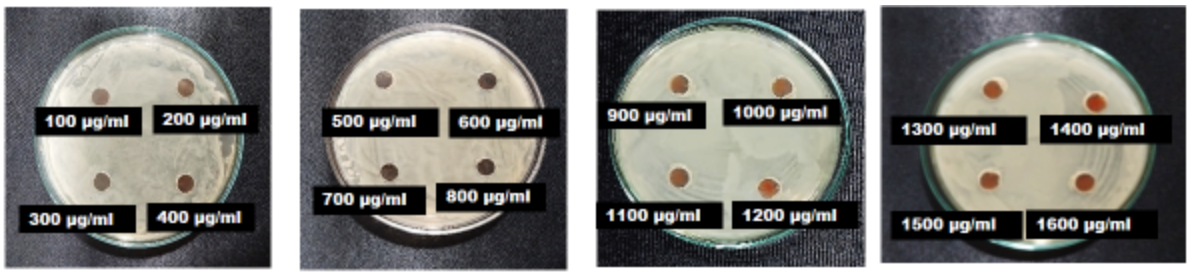


Figure 7

Well diffusion assay to analyze the antibacterial analysis of different concentrations of Fe-O-NP against TIU16A3 (accession number OR507186)

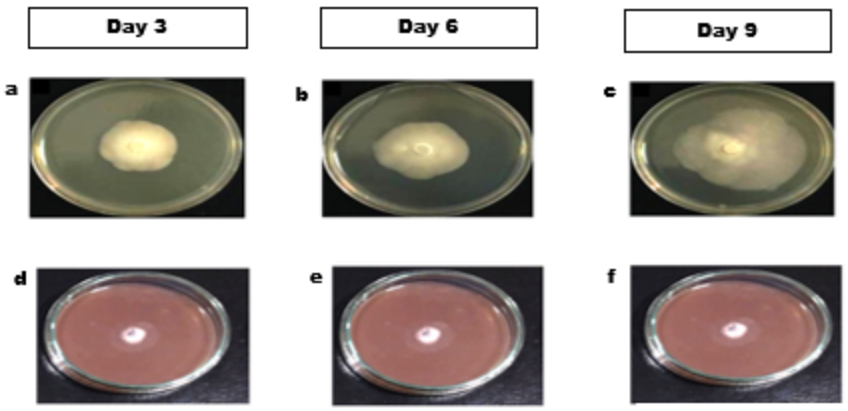


Figure 8

Growth of *Fusarium sp.* on Czapex dox agar Fig a, b, and c in absence of biogenic Fe-O-NP fig c, d, and e in the presence of biogenic Fe-O-NP.

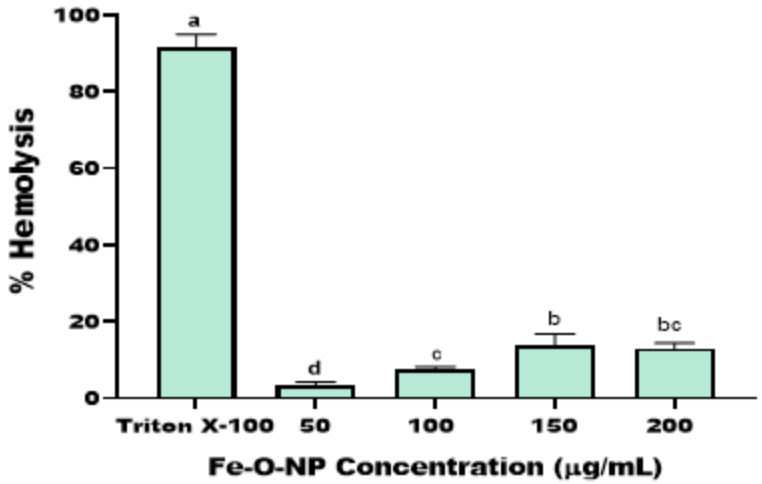


Figure 9

Hemolytic efficacy of biogenic Fe-O-NP at different concentrations. Similar alphabets in the plotting area depict no significance at P<0.05, and different alphabets in the plotting area depict significant differences in different treatment groups. Each value indicates the mean ± SE (*n* =3)

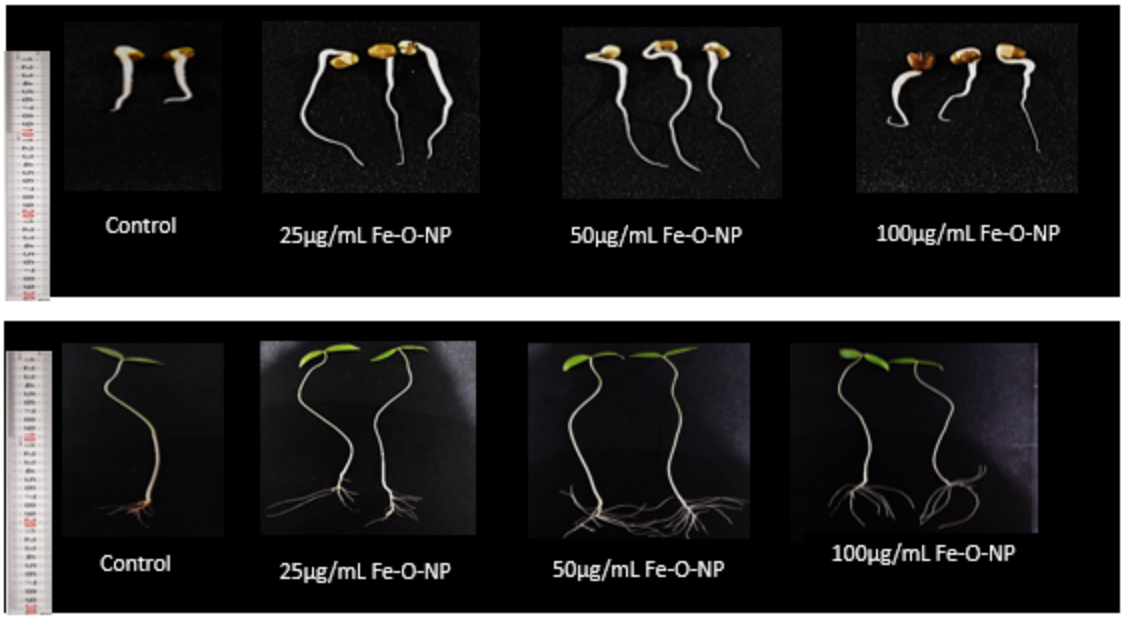


Figure 10

Effect of 25 µg/mL, 50 µg/mL, and 100 µg/mL Fe-O-NP on growth in *V. radiata* L.

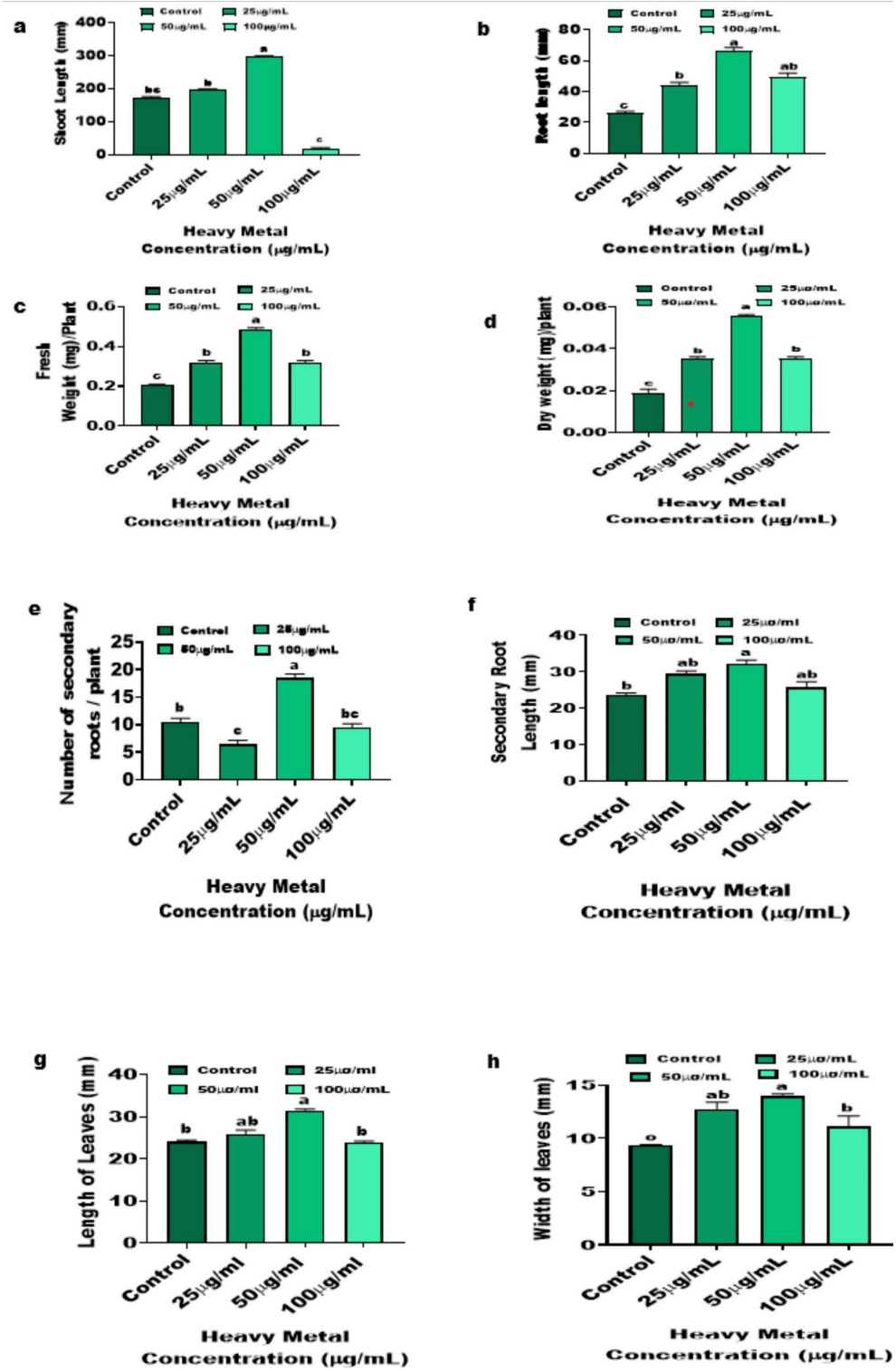


Figure 11

Effect of 25 µg/mL, 50 µg/mL, and 100 µg/mL Fe-O-NP on morpho-physiological parameters, shoot length, root length, fresh weight, dry weight, number of secondary roots, length of secondary root, leaves length, and leaves breadth in *V. radiata* L. . Similar alphabets in plotting area depict no significance at P<0.05, and different alphabets in plotting area depict significant difference in different treatment groups. Each value indicates the mean ± SE (*n* =15)

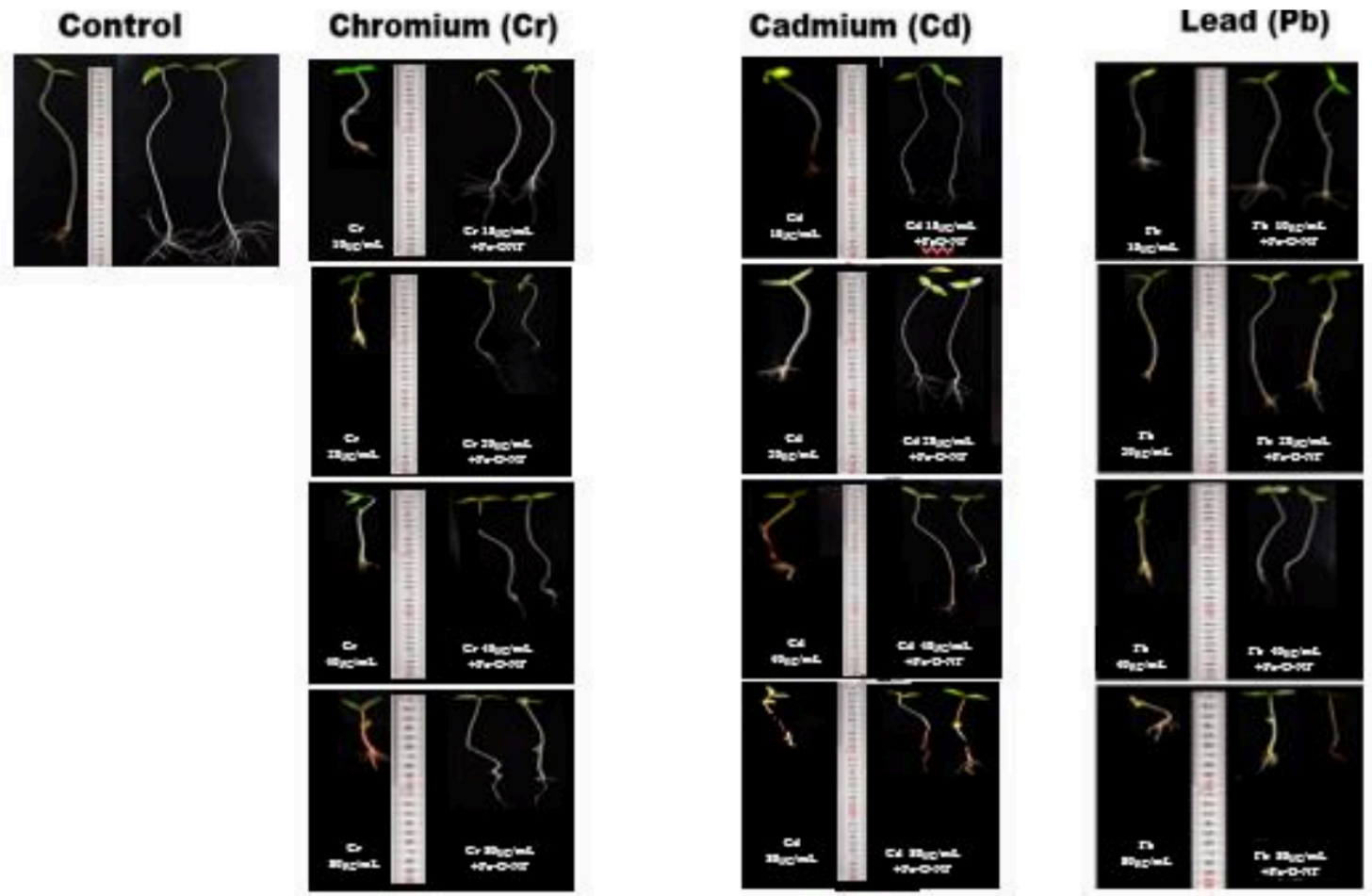


Figure 12

Plant body exhibiting detrimental effect of Cd, Cr and Pb stress on phenotypic variation in *Vigna radiata* L. Recovery of phenotypic traits of plants treated with Fe-O-NP (50 µg/mL).

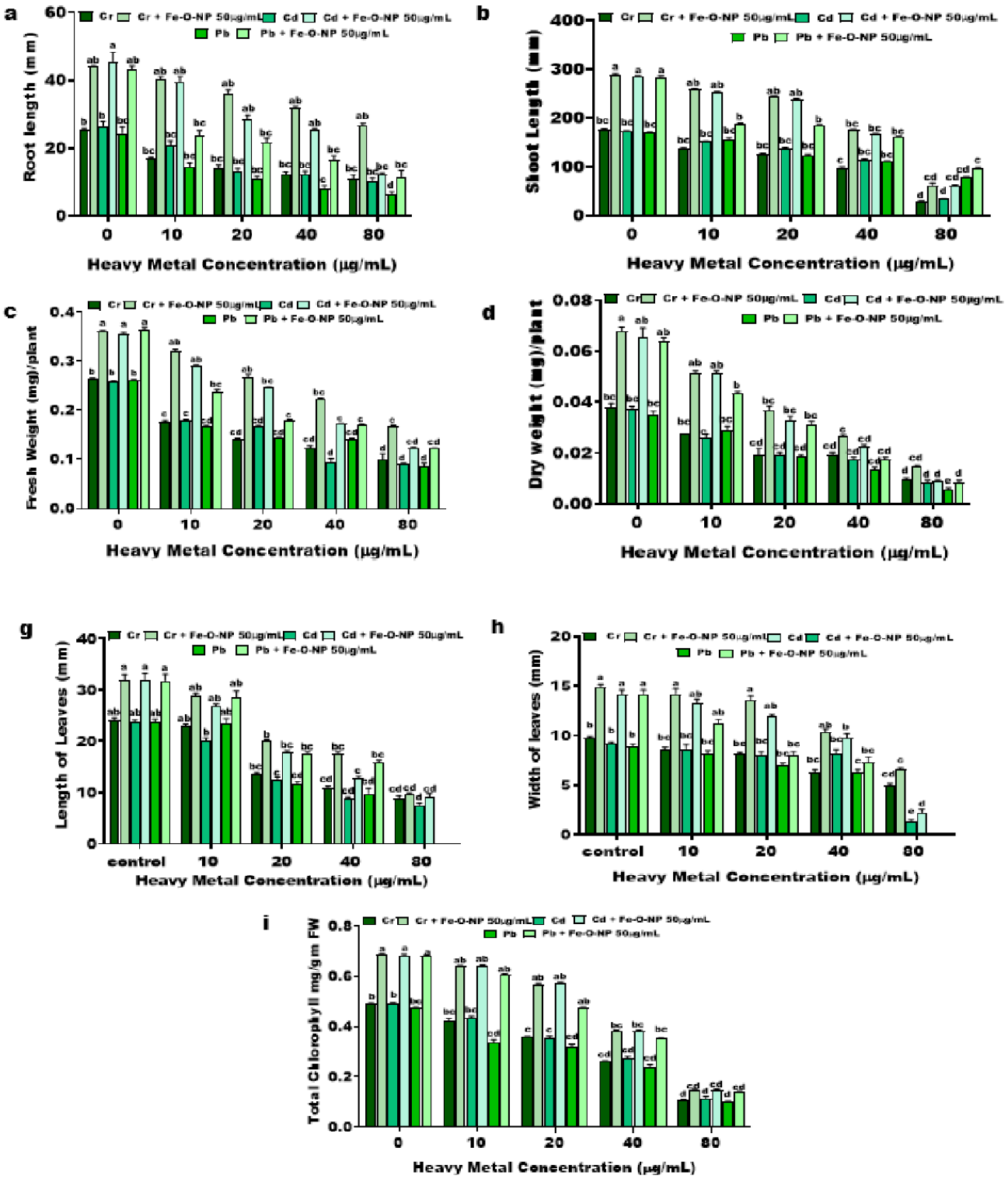


Figure 13

Effect of standardized Fe-O-NP on morpho-physiological parameters in *V. radiata* L. under different concentrations of Cd, Cr, and Pb stress. (a)-(g) HM induced deterioration in different morphological parameters and Fe-O-NP induced recovery in root length, shoot length, fresh weight, dry weight, leaves length, leaves breadth, and chlorophyll content. Similar alphabets in plotting area depict no significance

at P<0.05, and different alphabets in plotting area depict significant difference in different treatment groups. Each value indicates the mean ± SE (*n* =15).

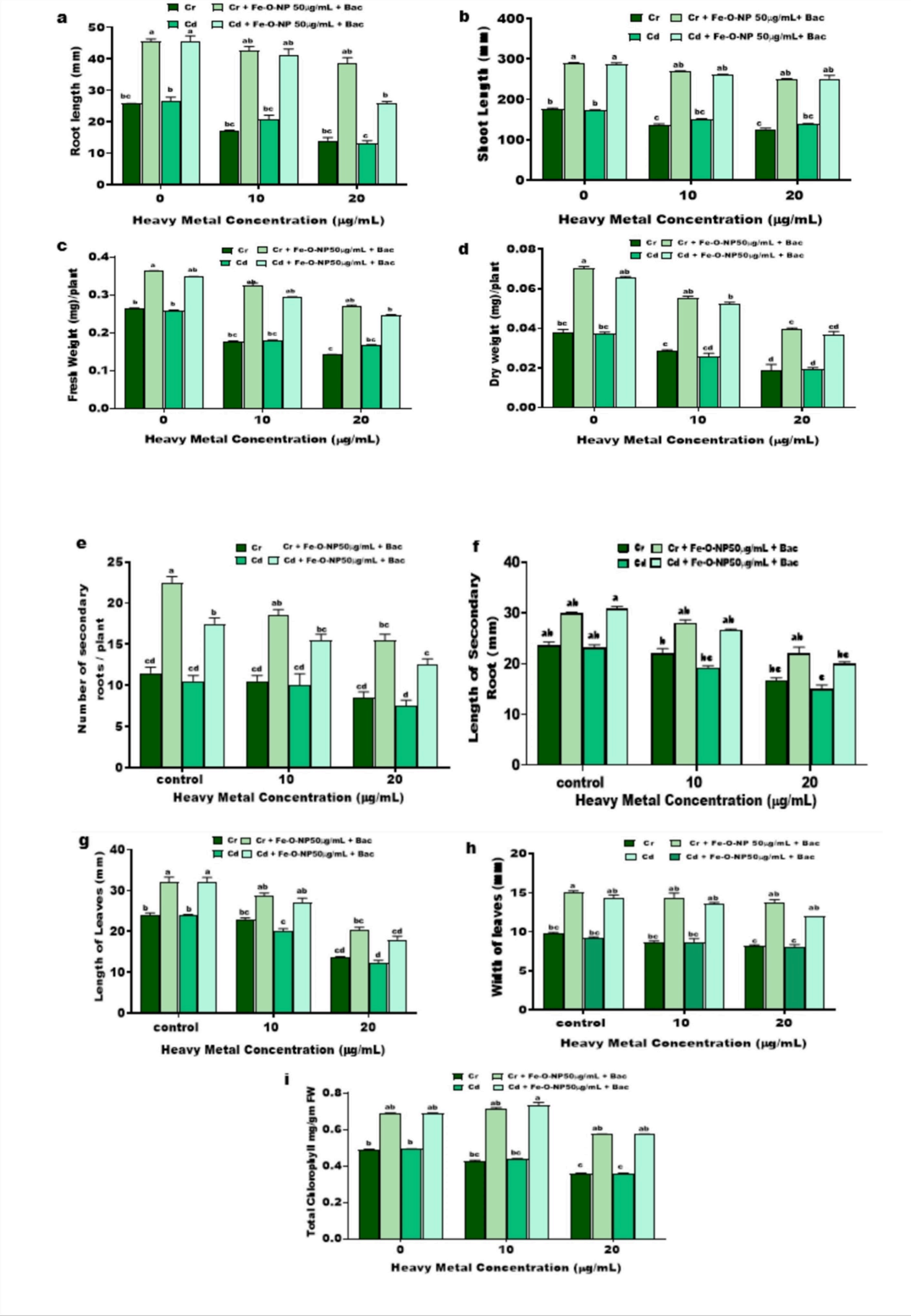


Figure 14

Effect of standardized Fe-O-NP + TIU16A3 on morpho-physiological parameters in *V. radiata* L. under different concentrations of Cd, and Cr stress. (a)-(i) HM induced deterioration in different morphological parameters and Fe-O-NP + TIU16A3 induced recovery in root length, shoot length, fresh weight, dry

weight, secondary root number, secondary root length, leaves length, leaves breadth, and total chlorophyll content. Similar alphabets in the plotting area depict no significance at P<0.05, and different alphabets in the plotting area depict significant differences in different treatment groups. Each value indicates the mean ± SE (*n* =15)

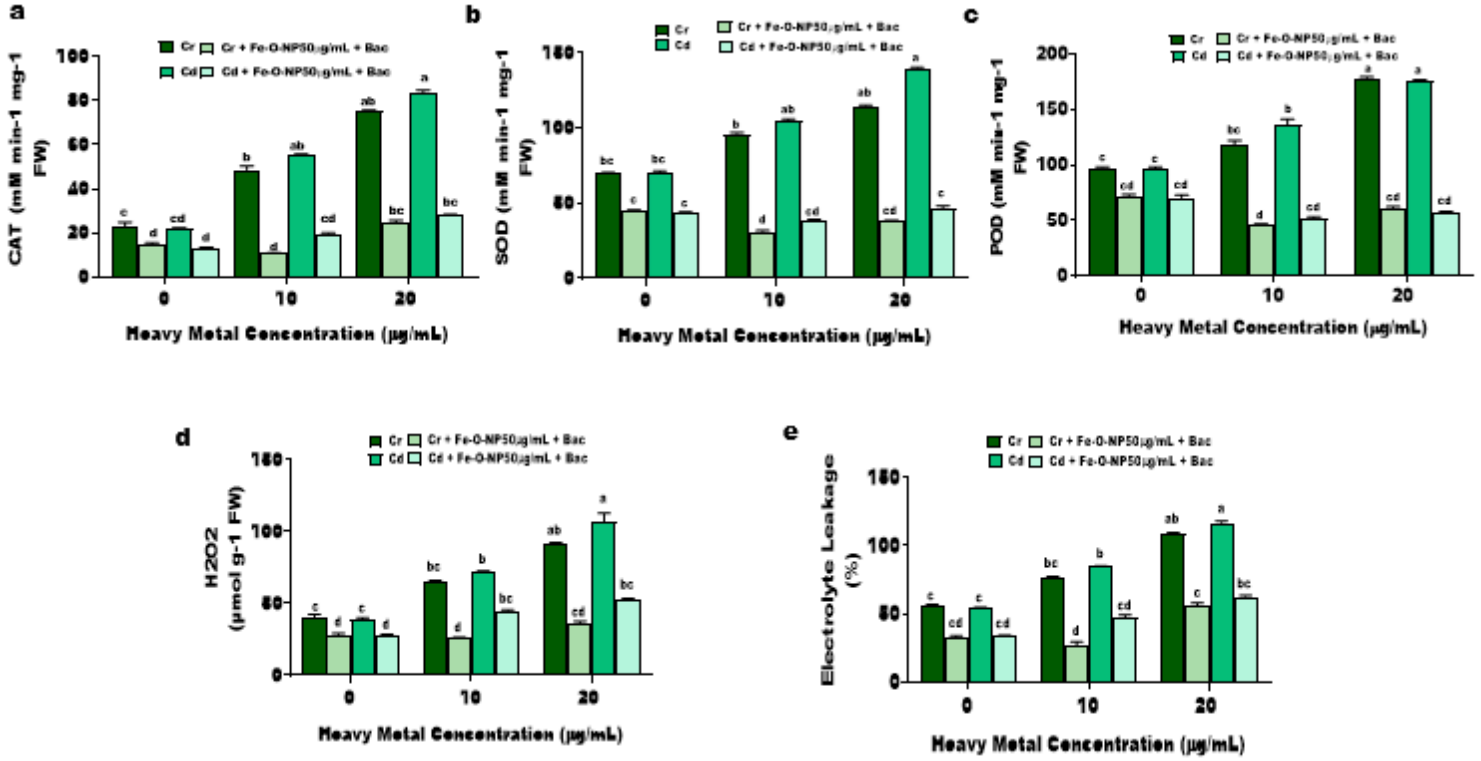


Figure 15

Effect of standardized Fe-O-NP + TIU16A3 on morpho-physiological parameters in *V. radiata* L. under different concentrations of Cd, and Cr stress. (a)-(e) HM induced deterioration in different morphological parameters and Fe-O-NP + TIU16A3 induced recovery in POD, CAT, SOD, H_2O_2, and EL % content. Similar alphabets in the plotting area depict no significance at P<0.05, and different alphabets in the plotting area depict significant differences in different treatment groups. Each value indicates the mean ± SE (*n* =15)

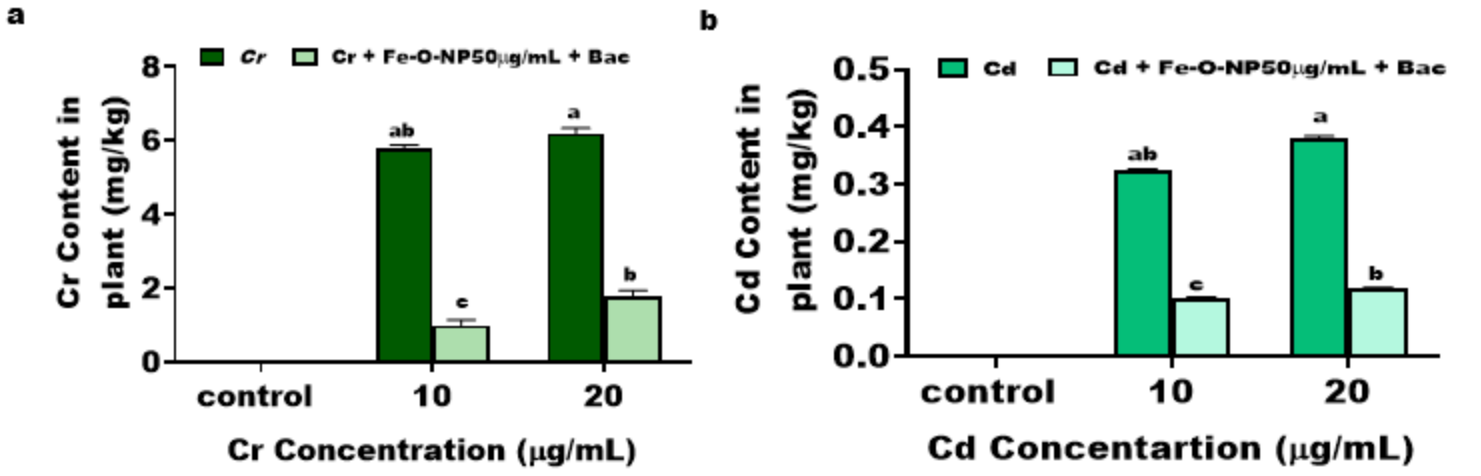


Figure 16

Flame Atomic absorption spectrophotometer analysis of heavy metal content in *V. radiata* L. Fig. a cadmium (Cd) content in TIU16A3 + 50 µg/mL Fe-O-NP treated plant. Fig. b chromium (Cr) content in TIU16A3 + 50 µg/mL Fe-O-NP treated plant. Similar alphabets in the plotting area depict no significance at P<0.05, and different alphabets in the plotting area depict significant differences in different treatment groups. Each value indicates the mean ± SE (*n* =15)

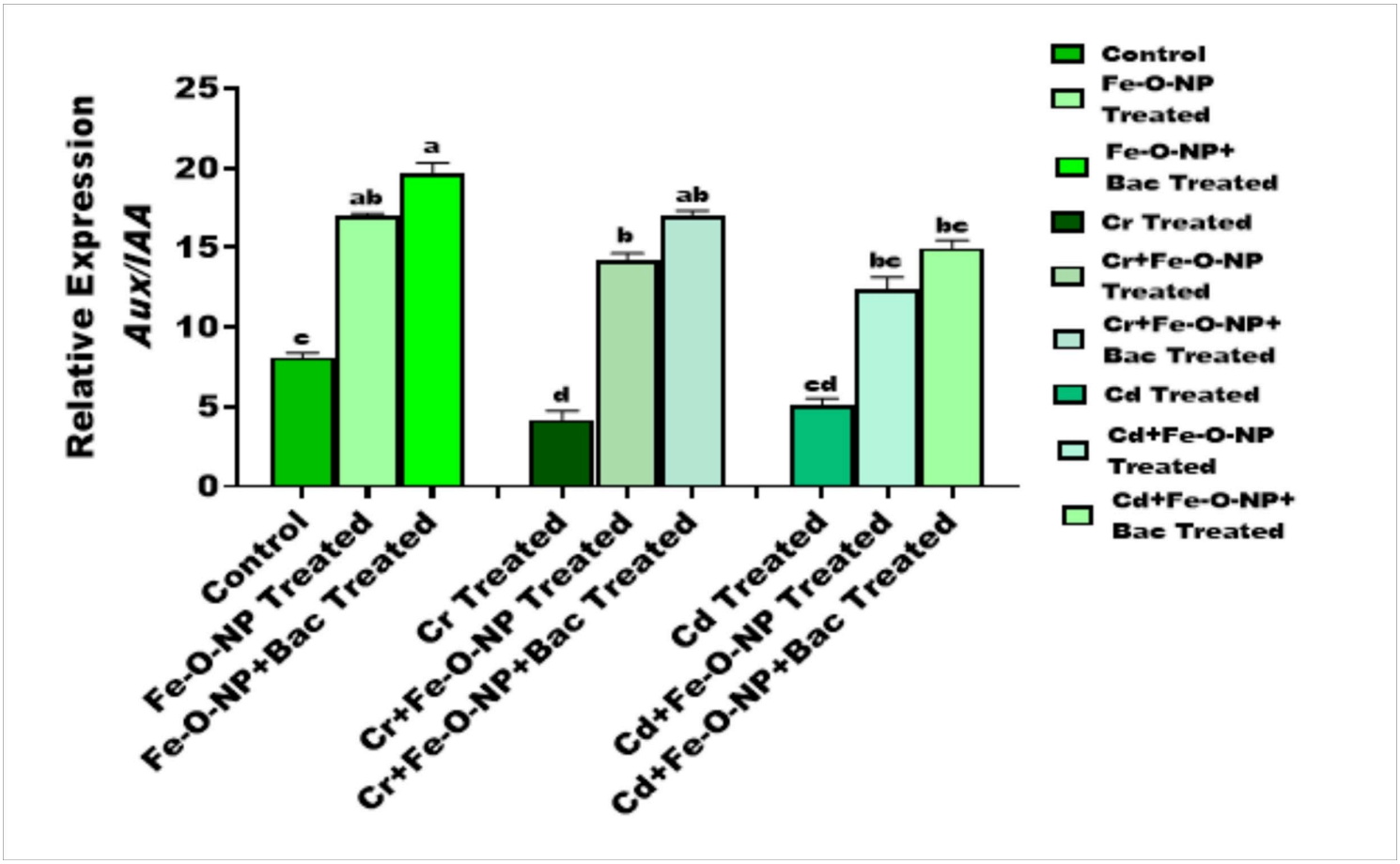


Figure 17

Gene expression analysis of *Aux/IAA* gene of *Vigna radiata* L. by RT-qPCR under the stress of heavy metals chromium (Cr), and cadmium (Cd) treated with Fe-O-NP (50 µg/mL) alone and Fe-O-NP (50 µg/mL) + TIU16A3. Similar alphabets in the plotting area depict no significance at P<0.05, and different alphabets in the plotting area depict significant differences in different treatment groups. Each value indicates the mean ± SE (*n* =15)